

# Mitigating the Modality Gap: Few-Shot Out-of-Distribution Detection with Multi-modal Prototypes and Image Bias Estimation

Yimu Wang, Evelien Riddell, Adrian Chow, Sean Sedwards, Krzysztof Czarnecki  
University of Waterloo

## Abstract

Existing vision-language model (VLM)-based methods for out-of-distribution (OOD) detection typically rely on similarity scores between input images and in-distribution (ID) text prototypes. However, the modality gap between image and text often results in high false positive rates, as OOD samples can exhibit high similarity to ID text prototypes. To mitigate the impact of this modality gap, we propose incorporating ID image prototypes along with ID text prototypes. We present theoretical analysis and empirical evidence indicating that this approach enhances VLM-based OOD detection performance without any additional training. To further reduce the gap between image and text, we introduce a novel few-shot tuning framework, SUPREME, comprising biased prompts generation (BPG) and image-text consistency (ITC) modules. BPG enhances image-text fusion and improves generalization by conditioning ID text prototypes on the Gaussian-based estimated image domain bias; ITC reduces the modality gap by minimizing intra- and inter-modal distances. Moreover, inspired by our theoretical and empirical findings, we introduce a novel OOD score  $S_{GMP}$ , leveraging uni- and cross-modal similarities. Finally, we present extensive experiments to demonstrate that SUPREME consistently outperforms existing VLM-based OOD detection methods.

## 1. Introduction

Detecting out-of-distribution (OOD) samples [12, 18, 21, 38, 41, 56, 60] is essential for the real-world deployment of machine learning models [16, 53, 65], as novel samples may emerge and should be flagged for careful consideration. Recently, inspired by the power of vision-language foundation models (VLMs) [14, 20, 53], novel approaches to OOD detection using VLMs [1, 2, 4, 11, 12, 24, 36, 40, 45, 46, 51, 61, 69] have gained significant attention. Early VLM-based OOD detection works [4, 24, 45, 61] mainly focus on using CLIP [53] in a zero-shot setting, where only the in-distribution (ID) class names are utilized. For example, Maximum Concept Matching (MCM) [45] measures

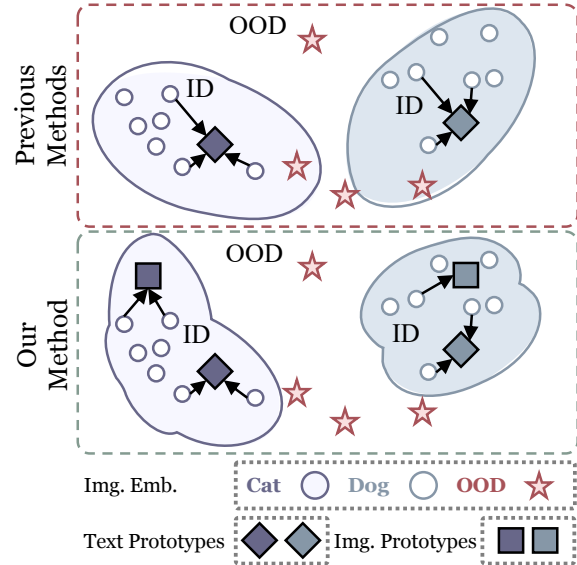


Figure 1. Standard VLM-based OOD detection methods [36, 45, 46] only utilize ID text prototypes ( $\diamond$ ) for identifying OOD samples. In comparison, SUPREME employs ID image prototypes ( $\square$ ) to complement ID text prototypes, reducing the impact of the image-text modality gap [39] and sharpening the boundary between ID and OOD data. “Img.” and “Emb.” represent image and embedding.

the similarity between input images and text embeddings of ID classes, also referred to as ID *text prototypes*, in the joint vision-language representation space of CLIP. MCM then uses this similarity score to differentiate OOD and ID samples, on the basis that ID samples should have higher similarity scores.

Following MCM, other zero-shot methods [4, 24, 61] aim at generating OOD text prototypes by querying large language models (LLMs) [26, 49] or WordNet [44]. These methods obtain OOD scores by evaluating the similarity difference between ID and OOD text prototypes. To further improve performance, various few-shot tuning OOD detection methods [2, 36, 40, 48, 69] have been proposed. These methods mainly target learning OOD (negative) text prototypes. For example, NegPrompt [36] learns OOD text

prototypes by minimizing the similarity between OOD text prototypes and ID data with contrastive learning.

While these approaches have shown promise using CLIP, they use only text prototypes and thus are limited by the modality gap [39] between image and text modalities. Liang *et al.* [39] demonstrate that CLIP’s image and text embeddings are located in two clearly separate regions of the embedding space. As a result, OOD images may also exhibit high similarity to ID text prototypes, since high similarity can stem from either true semantic similarity or mere spatial closeness to the ID text prototypes, causing a risk of increased false positives. This observation raises a critical question about the impact of the modality gap on VLM-based OOD detection, leading to our first research question:

*RQ1: What is the impact of the modality gap on VLM-based OOD detection methods?*

In response to RQ1, we hypothesize that the modality gap negatively impacts performance and that incorporating image and text (multi-modal) prototypes, as opposed to only text prototypes, could alleviate this effect. We illustrate this in Fig. 1. To explore this, we compute class-specific ID image prototypes by averaging embeddings extracted from the ID data within each class. We extend the MCM score  $S_{MCM}$  [45] to incorporate the image prototypes alongside the text prototypes. Compared to  $S_{MCM}$ , our empirical analysis shows that, without any training, using the extension of  $S_{MCM}$  with multi-modal prototypes improves average FPR95 and AUROC from 32.4 and 94.5 to 24.2 and 95.8, respectively, on Imagenet-100 [7] (ID) across four OOD datasets (Tab. 1). For theoretical support, in Theorem 1, we demonstrate that incorporating image prototypes increases the score separation between ID and OOD data, leading to improved performance.

Given these findings, *i.e.*, that the modality gap significantly affects VLM-based OOD detection, we conclude that it is necessary to explore approaches mitigating the gap to improve reliability. This leads us to our second research question:

*RQ2: How can we mitigate the impact of modality gap to improve VLM-based OOD detection?*

To address RQ2, we propose a novel few-Shot tuning, multi-modal **PR**ototype-based **ME**thod for OOD detection with CLIP, termed SUPREME. SUPREME comprises biased prompts generation (BPG) and image-text consistency (ITC) modules. BPG introduces a Gaussian-based image domain bias to enhance image-text fusion and improve generalization. ITC reduces the modality gap by minimizing inter- and intra-modal distances. SUPREME also makes use of a new OOD score, which we call the Generalized Multi-modal Prototype OOD score, denoted  $S_{GMP}$ .

**BPG.** To improve multi-modal fusion and generalization, in contrast to previous OOD detection methods [2, 36, 46] that only utilize learnable contexts for generating text prototypes, BPG conditions text prototypes on three components: learnable contexts, the image embedding, and the ID image domain bias. The image embedding and ID image domain bias facilitate image-text fusion, enhancing cross-modal alignment. The third component, the Gaussian-based ID image domain bias, captures the distribution of ID image embeddings to improve generalization.

**ITC.** To minimize the modality gap, we first map the image embedding  $I$  to the text domain as  $I' = f_{i2t}(I)$  with the image-to-text mapping  $f_{i2t}(\cdot)$ . To ensure it aligns with ID text prototypes, we introduce the inter-modal loss  $\ell_{inter}$ . Additionally, to avoid information loss, the intra-modal loss  $\ell_{intra}$  is applied between the original embedding  $I$  and the reconstructed image embedding  $\hat{I} = f_{t2i}(I')$  using the text-to-image mapping  $f_{t2i}(\cdot)$ .

**$S_{GMP}$ .** Building on our findings from RQ1, we introduce a new OOD score,  $S_{GMP}$ , which integrates uni- and cross-modal similarities. While previous methods rely solely on the similarity between ID text prototypes and input image embedding,  $S_{GMP}$  incorporates the similarity between multi-modal input embeddings—the image embedding  $I$  and the mapped image embedding  $f_{i2t}(I)$ —and ID multi-modal (image and text) prototypes, respectively. This allows  $S_{GMP}$  to balance inter- and intra-modal similarities, enhancing robustness and performance.

Our contributions are summarized as follows:

- (RQ1) We empirically and theoretically demonstrate that multi-modal (image and text) prototypes reduce the negative impact of the modality gap, resulting in performance improvements without additional training.
- (RQ2) To further mitigate the modality gap, we propose a novel few-shot tuning framework, SUPREME, comprising biased prompts generation (BPG) and image-text consistency (ITC) modules.
- (RQ2) Building on our empirical and theoretical results, we design a new OOD score,  $S_{GMP}$ , exploiting ID multi-modal prototypes and multi-modal input embeddings to enhance performance and robustness.
- (RQ2) Extensive experiments across multiple benchmarks, including ImageNet-1k [7], ImageNet-100 [7], ImageNet-10 [7], and ImageNet-20 [7], demonstrate that SUPREME outperforms existing OOD detection methods and achieves new state-of-the-art performance. We plan to release our code upon publication.

## 2. Related Work

**Out-of-distribution (OOD) detection.** OOD detection [18, 22, 41, 65, 68] aims to discriminate ID samples and OOD samples. Traditional methods include post-hoc [30, 50, 55, 56], confidence enhancement [9, 17, 47, 62, 64], and

outlier exposure methods [10, 12, 19, 21, 23, 28, 42, 71], by estimating the OOD probability using logits [18, 22, 38, 41] or feature representations [55, 60]. Recently, the field has shifted towards exploiting large-scale pre-trained VLMs [14, 20, 53], *i.e.*, CLIP [53], to enhance OOD detection, transitioning from uni-modal to multi-modal approaches. MCM [45] employs CLIP and explores the effects of softmax and temperature scaling in a zero-shot manner. Subsequent works can be roughly categorized into zero-shot and few-shot tuning methods. Zero-shot methods [4, 24, 45, 61] primarily focus on identifying negative classes by querying LLMs [26, 49] or WordNet [44]. In parallel, few-shot tuning methods [2, 36, 40, 48, 69] also mainly target finding negative text prompts (OOD text prototypes). For example, CATEX [40], LSN [48], and Neg-Prompt [36] learn negative prompts by minimizing the similarity between negative prompts and ID training data.

In contrast to previous VLM-based methods that use only text prototypes, SUPREME enhances OOD detection by employing multi-modal prototypes and encouraging cross-modal alignment to reduce the modality gap.

**Prompt tuning.** Prompt tuning originates in Natural Language Processing [31, 37, 54] as a method for automating template/prompt creation in models such as BERT [8] and GPT [49]. For example, AutoPrompt [54] is a gradient-based approach for identifying “optimal” prompts, replacing manually designed prompts. By adapting prompts in the input embedding space based on downstream data, prompt tuning offers a parameter-efficient alternative to fine-tuning. Recently, prompt tuning has been applied in computer vision models [27, 72, 73]. Notably, CoOp [73] and Co-CoOp [72], as representative methods in visual prompt tuning (VPT), employ learnable prompts optimized by minimizing classification loss to improve CLIP’s performance.

Different from previous VPT works [2, 40, 46, 48, 72, 73] that generate text prompts with text and individual image data, SUPREME generates text prompts/prototypes with a novel Gaussian-based image domain bias for estimating the distribution of image data, which enables enhanced image-text fusion with improved generalization ability.

### 3. Preliminaries

#### 3.1. Problem Setup

Let  $\mathcal{X}$  and  $\mathcal{Y} = \{y_1, \dots, y_C\}$  represent the feature space and ID label space, respectively, where  $C$  is the number of ID classes.

**OOD detection.** In real-world applications, AI models are trained on ID data and may misclassify OOD data into ID classes with high confidence [25]. To tackle this problem, OOD detection [66] is proposed to identify OOD samples using a score function  $S(\cdot)$  [33, 34]. A sample is classified as OOD if  $S(\mathbf{x}) \leq \gamma$ , where  $\gamma$  is a predefined threshold.

**Few-shot tuning.** In contrast to existing works that either utilize the entire ID training dataset [30, 35, 60] or avoid tuning entirely [4, 24, 45, 61], we study the scenario where the model is fine-tuned using only a subset of the ID training data (16 images per class) without access to OOD data or other additional data.

#### 3.2. Revisiting CLIP, MCM, and Prompt Tuning

**CLIP [53]** is a foundational VLM pre-trained on a web-scale image-text dataset using self-supervised contrastive learning [5], which achieves strong zero-shot classification results on numerous benchmark datasets [3, 29, 32, 43, 52]. Specifically, for classification, CLIP first incorporates class labels  $\mathcal{Y} = \{y_c\}_{c \in [C]}$ , *e.g.*, “cat” and “dog”, into fixed pre-designed, rather than learned, text prompts, *e.g.*, “a photo of a [CLASS]”. These prompts combined with class names are processed by CLIP’s text encoder  $f_{text}(\cdot)$  to generate text embeddings  $\{P_{t,c}\}_{c \in [C]}$ , where  $P_{t,c} = f_{text}(\text{a photo of a } y_c)$ . Given an image  $\mathbf{x}$ , the image embedding  $I$  is obtained by the image encoder  $f_{image}(\cdot)$  as  $I = f_{image}(\mathbf{x})$ . The predicted class label is  $\hat{y} = \arg \max_{c \in [C]} \cos(I, P_{t,c})$ , where  $\cos(\cdot, \cdot)$  denotes the cosine similarity. The zero-shot classification score is calculated as  $p = \text{Softmax}([\cos(I, P_{t,1}), \dots, \cos(I, P_{t,C})])$ , where  $\text{Softmax}(\cdot)$  is the softmax function.

**CLIP for OOD Detection (MCM) [45].** Beyond its strong classification capabilities, MCM demonstrates that pre-trained CLIP models also exhibit robust zero-shot OOD detection capabilities. Specifically, MCM defines the maximum classification score as the OOD score  $S_{MCM}$ ,

$$S_{MCM}(I, \{P_{t,c}\}_{c \in [C]}) = \max_{c \in [C]} \frac{\exp(\cos(I, P_{t,c})/\tau)}{\sum_{j \in [C]} \exp(\cos(I, P_{t,j})/\tau)}, \quad (1)$$

where  $\tau$  is the temperature, and  $\exp(\cdot)$  is the exponential function.

**Visual prompt tuning [15, 67, 72, 73].** To improve CLIP’s performance when target training data is accessible, CoOp [73] replaces manually designed prompt templates with learnable (soft) prompts as  $CoOp_c = [V_1, \dots, V_L, y_c]$ , where  $c \in [C]$ ,  $L$  is the length of learnable prompts, and each  $V_*$  represents a learnable vector. The class-wise text embedding is then generated as  $P_{t,c}^{CoOp} = f_{text}(CoOp_c), \forall c \in [C]$ . With CLIP’s text and image encoder parameters frozen, the learnable prompts are optimized using the cross-entropy loss,

$$\ell_{ID} = -\log \frac{\exp(\cos(I, P_{t,y}^{CoOp})/\tau)}{\sum_{c \in [C]} \exp(\cos(I, P_{t,c}^{CoOp})/\tau)}, \quad (2)$$

where  $y$  is the ground truth label for the input image. Following CoOp, to avoid potential overfitting on the training data, CoCoOp [72] conditions prompts on the image embedding  $I$  as  $CoCoOp_c = [V_1 + m(I), \dots, V_L + m(I), y_c]$ ,

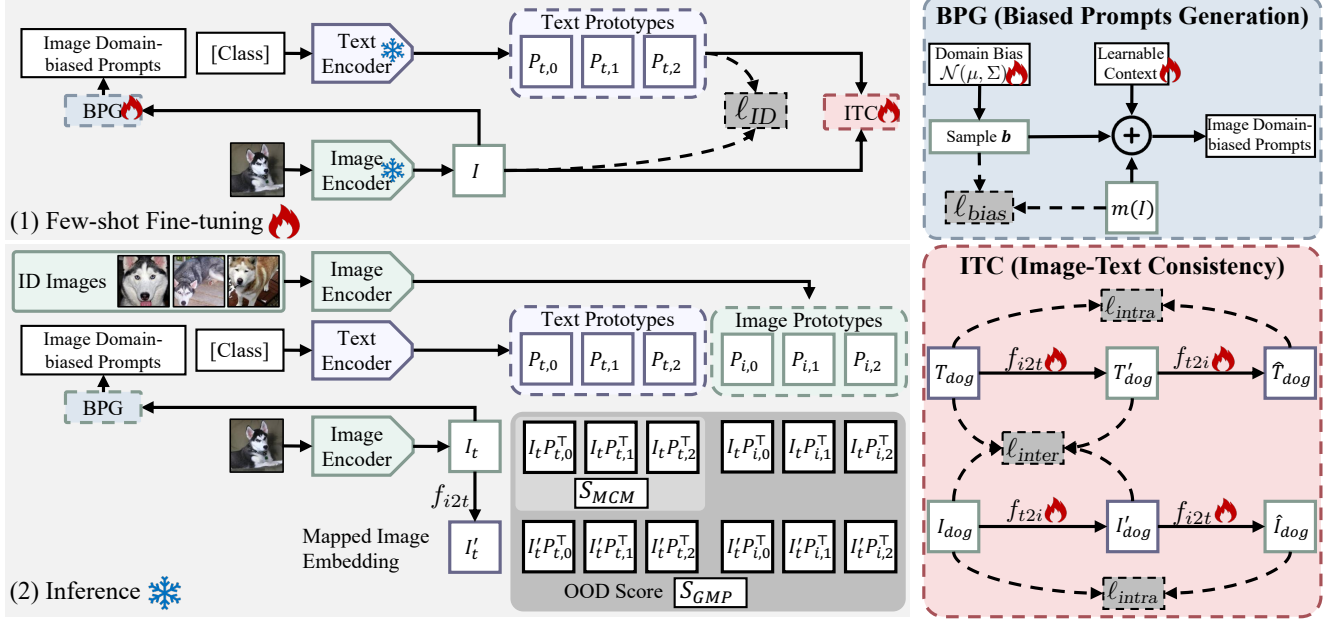


Figure 2. Overview of SUPREME. The two novel modules, *i.e.*, BPG (biased prompts generation) and ITC (image-text consistency), are designed to minimize the modality gap. 1) During the few-shot fine-tuning stage, BPG generates image domain-biased prompts, conditioned on the estimated image domain bias and the mapped image embedding  $m(I)$  for better image-text fusion. ITC minimizes the modality gap directly by the intra- and inter-modal losses ( $\ell_{intra}$  and  $\ell_{inter}$ ) with the text-to-image mapping  $f_{t2i}(\cdot)$  and the image-to-text mapping  $f_{i2t}(\cdot)$ . 2) During inference, image prototypes are obtained by averaging each class’s base ID image embeddings (Eq. (3)). The proposed  $S_{GMP}$  (Eq. (11)) is calculated based on the maximum similarity between the multi-modal embeddings (the image embedding  $I_t$  and mapped image embedding  $I'_t$ ) and ID multi-modal prototypes (*i.e.*, text prototypes  $\{P_{t,c}\}_{c \in [C]}$  and image prototypes  $\{P_{i,c}\}_{c \in [C]}$ ).  $S_{MCM}$  refers to the MCM score [45].

where  $m(\cdot)$  is a two-layer multi-layer perception (MLP, Linear-ReLU-Linear).

## 4. Methodology

In this section, we first answer RQ1 by presenting our hypothesis and findings in Sec. 4.1, where we demonstrate that the modality gap negatively impacts performance and that incorporating image prototypes alleviates this effect. Then, to mitigate the modality gap (RQ2), we introduce SUPREME in Sec. 4.2 with two modules and a novel OOD score,  $S_{GMP}$ , as shown in Fig. 2. Note that in this section, we denote the input image embedding by  $I_t$ .

### 4.1. RQ1: Multi-modal Prototypes

CLIP has been widely applied in different areas [13, 58]. However, a recent study [39] demonstrates that representations of images and texts are clearly separated, creating what is known as the modality gap. It remains unclear, however, whether this modality gap positively or negatively impacts OOD detection.

We hypothesize that the modality gap negatively impacts OOD detection performance by causing misalignment between image and text embeddings, and that this misalignment can lead to increased false positives, as OOD images

may exhibit high similarity to ID text prototypes due to either semantic similarity or small spatial distance.

To test our hypothesis, we demonstrate that incorporating multi-modal (image and text) prototypes can mitigate the negative impact of the modality gap and reduce false positives. We obtain ID text prototypes  $\{P_{t,c}\}_{c \in [C]}$  as in MCM [45]. For ID image prototypes  $\{P_{i,c}\}_{c \in [C]}$ , we collect ID base images  $\mathcal{X}_{base} = \{\mathbf{x}_i\}_{i \in [N_{base}]}$  with corresponding labels  $\{y_{base,i}\}_{i \in [N_{base}]}$ , where  $N_{base}$  is the number of base images. ID image prototypes are then calculated by averaging the image embeddings for each class,

$$P_{i,c} = \frac{\sum_{i \in [N_{base}]} \mathbb{I}(y_{base,i} = c) f_{image}(\mathbf{x}_i)}{\sum_{j \in [N_{base}]} \mathbb{I}(y_{base,j} = c)}, \forall c \in [C], \quad (3)$$

where  $\mathbb{I}(\cdot)$  is the indicator function and  $f_{image}(\cdot)$  is CLIP’s image encoder. With these image prototypes, we extend  $S_{MCM}$  (Eq. (1)) [45] to a new OOD score, termed the Multi-Modal Prototypes score,  $S_{MMP}$ , defined as,

$$S_{MMP} = \frac{S_{MCM}(I_t, \{P_{i,c}\}_{c \in [C]}) + S_{MCM}(I_t, \{P_{t,c}\}_{c \in [C]})}{2}. \quad (4)$$

This approach balances contributions from both modalities, potentially mitigating the impact of the modality gap.

**Empirical evidence.** We begin by empirically validating the effectiveness of image prototypes and  $S_{MMP}$ . We

Methods	FPR95 (%) ↓	AUROC (%) ↑
ImageNet-100 → 4 Datasets (Average)		
$S_{MCM}$ [45]	32.58	94.48
$S_{MMP}$ (Ours, Eq. (4))	<b>24.18</b>	<b>95.79</b>

Table 1. Comparison of OOD detection results on ImageNet-100 (ID) → 4 OOD datasets (OOD). We use CLIP-B/16 for  $S_{MCM}$  and  $S_{MMP}$ . FPR95 represents the false positive rate of OOD images when the true positive rate of ID images is at 95%. AUROC is the area under the receiver operating characteristic curve. Best in **bold**. Full results are in the Appendix.

use ImageNet-100 [7] as the ID dataset, with four OOD datasets: iNaturalist [59], SUN [63], Places [70], and Texture [6]. With all training images of ImageNet-100 as the base set, we observe in Tab. 1 that, on average,  $S_{MMP}$  outperforms  $S_{MCM}$  in both FPR95 and AUROC, demonstrating the effectiveness of image prototypes and  $S_{MMP}$ .

**Theoretical evidence.** To further demonstrate why image prototypes improve performance, we present a theoretical justification in Theorem 1. The theorem shows that  $S_{MMP}$  increases the expected score separation between ID and OOD samples compared to using text prototypes alone as in  $S_{MCM}$ . The proof is presented in the Appendix.

**Theorem 1** (Multi-modal Prototypes Increase Score Separation between ID and OOD Data). *Assuming that the OOD data is not drawn from any ID distribution, we have,*

$$\mathbb{E}[S_{MMP}(I_{ID}) - S_{MMP}(I_{OOD})] \geq \mathbb{E}[S_{MCM}(I_{ID}) - S_{MCM}(I_{OOD})], \quad (5)$$

where  $I_{ID}$  and  $I_{OOD}$  are the image embeddings of ID and OOD samples. We omit multi-modal prototypes for clarity.

While incorporating image prototypes improves performance both empirically and theoretically, inspired by recent research [36, 46], we further fine-tune CLIP in a few-shot tuning manner to mitigate the impact of the modality gap (RQ2). The details are presented in the following section.

## 4.2. RQ2: SUPREME

To alleviate the negative impact of the image-text modality gap [39] in CLIP (RQ2), we propose SUPREME, which is summarized in Fig. 2. SUPREME incorporates two novel modules, *i.e.*, the biased prompts generation module (BPG) and the image-text consistency module (ITC), along with a new OOD score. BPG enhances image-text fusion using image domain-biased prompts, while ITC minimizes both intra- and inter-modal distances. SUPREME’s novel OOD score,  $S_{GMP}$ , leverages uni- and cross-modal similarities for improving robustness and performance.

**Biased Prompts Generation (BPG).** Drawing inspiration from CoCoOp [73], we employ a set of learnable contexts  $\{V_i\}_{i \in [L]}$  and the mapped image embedding  $m(I_t)$  to

generate the text prototypes, where  $L$  is the length of learnable contexts and  $m(\cdot)$  is a two-layer MLP.

To enhance image-text fusion and improve generalization, we introduce a third component, a Gaussian-based estimated image domain bias  $\mathcal{N}(\mu, \Sigma)$ , for generating the prompts and ID text prototypes. This bias models the distribution of the mapped ID image embeddings, enabling the model to better distinguish between ID and OOD samples during inference. After that, we generate image domain-biased prompts (IDBP) conditioned on these three components. We next introduce the details of estimating the bias and generating IDBP.

**Estimating image domain bias.** In each training iteration, we sample  $\mathbf{b}$  from the Gaussian-based image domain bias  $\mathcal{N}(\mu, \Sigma)$  as,

$$\mathbf{b} = \mu + \sigma n, n \sim \mathcal{N}(0, \mathcal{I}), \quad (6)$$

where  $\Sigma = \sigma\sigma^\top$  (based on the Cholesky decomposition) and  $\mathcal{N}(0, \mathcal{I})$  represents the standard Gaussian distribution, given identity matrix  $\mathcal{I}$ . To align the domain bias with the distribution of training ID image embeddings, we employ the following loss,

$$\ell_{bias} = \|\mu - m(I_t)\|_1 + \|\mathbf{b} - m(I_t)\|_1, \quad (7)$$

where  $\|\cdot\|_1$  is the  $\ell_1$  distance.

**Generating image domain-biased prompts (IDBP).** We condition our IDBP on three components: the learnable contexts  $\{V_i\}_{i \in [L]}$ , mapped image embedding  $m(I_t)$ , and a sample  $\mathbf{b}$  from the estimated domain bias  $\mathcal{N}(\mu, \Sigma)$  as,

$$IDBP_c = [V_1 + m(I_t) + \mathbf{b}, \dots, V_L + m(I_t) + \mathbf{b}, y_c]. \quad (8)$$

The final ID text prototype  $P_{t,c}$  for the  $c$ -th class is obtained as  $P_{t,c} = f_{text}(IDBP_c)$ .

We thus establish a foundation for cross-modal fusion by conditioning prompts on learned contexts, image embeddings, and the estimated image domain bias.

**Image-Text Consistency (ITC).** While BPG reduces the gap by image-text fusion, image-text consistency (ITC) directly reduces the modality gap by aligning image and text embeddings through inter- and intra-modal distances at a fine-grained level. It consists of two mappings, *i.e.*, the image-to-text mapping  $f_{i2t}(\cdot)$  and text-to-image mapping  $f_{t2i}(\cdot)$ , which are used for mapping embeddings into another domain/modality.

The first component of ITC is the *inter-modal loss*. It is designed to ensure that mapped text/image embeddings ( $f_{t2i}(P_{t,c}), \forall c \in [C]$  and  $f_{i2t}(I_t)$ ) remain close to their original counterparts, thus enabling effective alignment. It is designed to minimize the cross-entropy loss,

$$\ell_{inter} = -\log \frac{\exp(\cos(I_t, f_{t2i}(P_{t,y}))/\tau)}{\sum_{c \in [C]} \exp(\cos(I_t, f_{t2i}(P_{t,c}))/\tau)} \quad (9)$$

$$- \log \frac{\exp(\cos(f_{i2t}(I_t), P_{t,y})/\tau)}{\sum_{c \in [C]} \exp(\cos(f_{i2t}(I_t), P_{t,c})/\tau)},$$

where  $y$  is the ground truth label for the input image,  $C$  is the number of classes, and  $\tau$  is the temperature.

Next, to prevent information loss, we introduce *intra-modal loss*. Specifically, we reconstruct the original embedding by mapping the mapped embedding back to its initial modality. Then, we minimize the  $\ell_1$  distance between the reconstructed and original embeddings as follows,

$$\begin{aligned} \ell_{intra} = & \|I_t - f_{t2i}(f_{i2t}(I_t))\|_1 \\ & + \sum_{c \in [C]} \|P_{t,c} - f_{i2t}(f_{t2i}(P_{t,c}))\|_1. \end{aligned} \quad (10)$$

The inter- and intra-modal losses serve to reduce the modality gap between image and text, and to preserve all information during mapping. To avoid overfitting, instead of using deep MLPs, we employ linear transformations without bias as the mappings ( $f_{i2t}(\cdot)$  and  $f_{t2i}(\cdot)$ ).

Combining BPG with ITC, SUPREME mitigates the modality gap by enhancing image-text fusion (BPG) as well as reducing inter- and intra-modal distances (ITC).

**Training, Inference, and  $S_{GMP}$ .** Our overall training objectives are a linear combination of the four losses:  $\mathcal{L} = \ell_{ID} + \alpha(\ell_{intra} + \ell_{inter}) + \beta\ell_{bias}$ , where  $\alpha$  and  $\beta$  are trade-off parameters. During inference, we use the mean  $\mu$  of the image domain bias as the sample  $\mathbf{b}$  to generate image domain-biased prompts.

**Generalized multi-modal prototypes OOD score  $S_{GMP}$ .** Building on our empirical and theoretical findings in Sec. 4.1, with the image-to-text mapping  $f_{i2t}(\cdot)$ , we introduce the generalized multi-modal prototypes OOD score  $S_{GMP}$ .  $S_{GMP}$  uses the average of the maximum similarities between the multi-modal input embedding (the image embedding  $I_t$  and mapped image embedding  $I'_t = f_{t2i}(I_t)$ ) and multi-modal prototypes:

$$\begin{aligned} & S_{GMP}(I_t, I'_t, \{P_{t,c}\}_{c \in [C]}, \{P_{i,c}\}_{c \in [C]}) \\ = & \frac{1}{4}(S_{MCM}(I_t, \{P_{t,c}\}_{c \in [C]}) + S_{MCM}(I_t, \{P_{i,c}\}_{c \in [C]}) \\ & + S_{MCM}(I'_t, \{P_{t,c}\}_{c \in [C]}) + S_{MCM}(I'_t, \{P_{i,c}\}_{c \in [C]})). \end{aligned} \quad (11)$$

**Remark.**  $S_{GMP}$  extends  $S_{MCM}$  by incorporating both uni- and cross-modal similarities.  $S_{GMP}$  balances contributions from both modalities, thus mitigating the negative impact of the modality gap. This approach enhances the separation between ID and OOD samples, improving the OOD detection performance of VLM-based methods as shown in Fig. 5.

## 5. Experiments

### 5.1. Experimental Details

**Datasets and benchmarks.** Our experiments primarily use the ImageNet-1k [7] and ImageNet-100 [7] dataset as ID data. Aligning with standards from prior works [45, 61], we evaluate on four diverse OOD datasets: iNaturalist [59], SUN [63], Places [70], and Texture [6]. Additionally, we test on ImageNet-10 [7] and ImageNet-20 [7] for near OOD. Details are in the Appendix.

**Baselines methods.** We compare SUPREME with 19 baseline methods, including traditional OOD detection methods [12, 18, 21, 38, 41, 56, 60], VLM (CLIP)-based OOD methods [2, 4, 24, 36, 40, 45, 46, 48, 57, 61], and visual prompt tuning methods [72, 73].

**Implementation details.** All the images in the official training set are used to obtain ID image prototypes. For each class, 16 images are used for few-shot tuning. We use the image and text encoders of VIT-B/16 pre-trained by CLIP [53] for all the experiments. The parameters of CLIP are frozen. We use SGD to optimize other parameters, *e.g.*, estimated image domain bias and learnable context, with a momentum of 0.9. Training epochs, learning rate, batch size, and learnable context length are set to 50, 0.002, 32, and 16, respectively. We set  $\alpha = 0.005$  and  $\beta = 0.1$ . Experiments are conducted on a single Nvidia V100 with 32 GB memory. All the reported results for SUPREME are the average of three trials.

**Metrics.** We employ two widely accepted metrics: FPR95, the false positive rate of OOD images when the true positive rate of ID images is at 95%, and AUROC, the area under the receiver operating characteristic curve.

### 5.2. Main Results

**ImageNet-1k and ImageNet-100 as the ID dataset.** In Tab. 2, we present a comprehensive analysis on ImageNet-1k (ID) across four OOD datasets (iNaturalist, SUN, Places, Texture) using CLIP (VIT-B/16). SUPREME demonstrates superior performance, achieving the lowest FPR95 and highest AUROC scores across most datasets. Notably, SUPREME achieves an average FPR95 of 20.28 and an average AUROC of 95.54. In Tab. 3, we observe consistent trends using ImageNet-100 as the ID dataset. SUPREME achieves the best average results, with FPR95 of 8.19 and AUROC of 98.08, showing substantial improvements over other methods. These results underscore our method’s robustness across varied OOD benchmark datasets, emphasizing its effectiveness in enhancing model reliability for real-world applications. However, we note that these OOD datasets are mostly semantically different from the ID data (ImageNet), making this problem easier. To evaluate SUPREME under more challenging conditions (near OOD), we follow previous work [24, 45] and conduct experiments

Methods	Venue	ImageNet-1k $\rightarrow$ OOD Datasets								Average	
		iNaturalist		SUN		Places		Texture			
		FPR95 $\downarrow$	AUROC $\uparrow$	FPR95 $\downarrow$	AUROC $\uparrow$	FPR95 $\downarrow$	AUROC $\uparrow$	FPR95 $\downarrow$	AUROC $\uparrow$	FPR95 $\downarrow$	AUROC $\uparrow$
MOS $\dagger$ [21] (BiT)	CVPR'21	9.28	98.15	40.63	92.01	49.54	89.06	60.43	81.23	39.97	90.11
Fort <i>et al.</i> $\dagger$ [12] (ViT-B)	NeurIPS'21	15.07	96.64	54.12	86.37	57.99	85.24	53.32	84.77	45.12	88.25
Energy $\dagger$ [41] (ViT-B)	NeurIPS'20	21.59	95.99	34.28	93.15	36.64	91.82	51.18	88.09	35.92	92.26
MSP $\dagger$ [18] (ViT-B)	ICLR'17	40.89	88.63	65.81	81.24	67.90	80.14	64.96	78.16	59.89	82.04
ODIN $\ddagger$ [38]	ICLR'18	30.22	94.65	54.04	87.17	55.06	85.54	51.67	87.85	47.75	88.80
ViM $\ddagger$ [60]	CVPR'22	32.19	93.16	54.01	87.19	60.67	83.75	53.94	87.18	50.20	87.82
KNN $\ddagger$ [56]	ICML'22	29.17	94.52	35.62	92.67	39.61	91.02	64.35	85.67	42.19	90.97
VLM-based OOD Detection (CLIP of ViT-B/16)											
MCM [45]	NeurIPS'22	30.91	94.61	37.59	92.57	44.69	89.77	57.77	86.11	42.74	90.77
CoOp* [73]	IJCV	29.47	94.89	31.34	93.36	40.28	90.07	54.25	87.58	38.83	91.47
CoCoOp* [72]	CVPR'22	30.74	94.73	31.18	93.15	38.75	90.63	53.84	87.92	38.63	91.61
NPOS [57]	ICLR'23	16.58	96.19	43.77	90.44	45.27	89.44	46.12	88.80	37.93	91.22
LoCoOp [46]	NeurIPS'23	16.05	96.86	23.44	95.07	32.87	91.98	42.28	90.19	28.66	93.52
CATEX [40]	NeurIPS'23	10.18	97.88	33.87	92.83	41.43	90.48	33.17	92.73	29.66	93.48
CLIPN [61]	CVPR'23	23.94	95.27	26.17	93.93	33.45	92.28	40.83	90.93	31.10	93.10
NegLabel [24]	ICLR'24	<b>1.91</b>	<b>99.49</b>	20.53	95.49	35.59	91.64	43.56	90.22	25.40	94.21
LSN [48]	ICLR'24	21.56	95.83	26.32	94.35	34.48	91.25	38.54	90.42	30.22	92.96
EOE [4]	ICML'24	12.29	97.52	20.40	95.73	30.16	92.95	57.53	85.64	30.09	92.96
ID-Like (4-shots) [2]	CVPR'24	8.98	98.19	42.03	91.64	44.00	90.57	<b>25.27</b>	94.32	30.07	93.68
NegPrompt [36]	CVPR'24	6.32	98.73	22.89	95.55	27.60	93.34	35.21	91.60	23.01	94.81
<b>SUPREME</b>		<b>8.27</b>	<b>98.29</b>	<b>19.40</b>	<b>95.84</b>	<b>26.69</b>	<b>93.56</b>	26.77	<b>94.45</b>	<b>20.28</b>	<b>95.54</b>

Table 2. OOD detection results with ID data of ImageNet-1k and four OOD datasets using CLIP (ViT-B/16). Best in **Bold**. “\*” is cited from LSN [48]. “ $\dagger$ ” represents results from MCM [45]. “ $\ddagger$ ” represents results from NPOS [57].

Methods	ImageNet-100 $\rightarrow$ OOD Datasets								Average	
	iNaturalist		SUN		Places		Texture			
	FPR95 $\downarrow$	AUROC $\uparrow$	FPR95 $\downarrow$	AUROC $\uparrow$	FPR95 $\downarrow$	AUROC $\uparrow$	FPR95 $\downarrow$	AUROC $\uparrow$	FPR95 $\downarrow$	AUROC $\uparrow$
MSP $\dagger$	23.55	95.92	37.02	92.45	40.76	91.23	24.40	94.90	31.43	93.63
ViM $\dagger$	20.11	96.22	38.56	93.12	44.01	87.33	33.12	93.24	33.95	92.48
MCM	18.13	96.77	36.45	94.54	34.52	94.36	41.22	92.25	32.58	94.48
CoOp $\dagger$	9.30	97.95	11.64	97.61	17.45	96.53	15.94	96.90	13.58	97.25
CoCoOp $\dagger$	11.76	97.84	14.28	97.13	15.16	96.73	18.27	96.54	14.86	97.06
LSN	4.93	98.92	8.23	<b>98.98</b>	12.82	<b>97.19</b>	<b>8.26</b>	<b>98.11</b>	8.56	98.05
<b>SUPREME</b>	<b>2.54</b>	<b>99.21</b>	<b>8.08</b>	98.28	<b>12.17</b>	97.15	9.98	97.69	<b>8.19</b>	<b>98.08</b>

Table 3. OOD detection results with ID data of ImageNet-100 and four OOD datasets using CLIP (ViT-B/16). Best in **Bold**. “ $\dagger$ ” represents results from LSN [48].

Methods	ImageNet-10 $\rightarrow$ ImageNet-20		ImageNet-20 $\rightarrow$ ImageNet-10	
	FPR95 (%) $\downarrow$	AUROC (%) $\uparrow$	FPR95 (%) $\downarrow$	AUROC (%) $\uparrow$
Energy $\dagger$	10.30	97.94	16.40	97.37
CLIPN $\dagger$	7.80	98.07	13.67	97.47
MCM $\dagger$	5.00	98.71	17.40	98.87
LoCoOp*	5.60	98.47	5.40	98.92
NegLabel	5.10	98.86	4.60	98.81
<b>SUPREME</b>	<b>4.00</b>	<b>98.93</b>	<b>3.80</b>	<b>98.98</b>

Table 4. Comparison on ImageNet-10  $\leftrightarrow$  ImageNet-20. We use CLIP-B/16 for all the experiments. Best in **bold**. “\*” represents our reproduction. “ $\dagger$ ” refers to results from EOE [4].

Methods	FPR95 $\downarrow$	AUROC $\uparrow$	Methods	Top-1 Acc. (%)
<b>SUPREME</b>	<b>20.28</b>	<b>95.54</b>	MCM	67.0
- BPG	27.51	93.71	CLIPN	68.5
- ITC	28.59	93.38	ID-like	68.3
- $S_{GMP}$	25.03	94.80	<b>SUPREME</b>	<b>71.8</b>

Table 5. Effectiveness of different modules and the proposed OOD score  $S_{GMP}$ .

Table 6. Comparison in ID accuracy on ImageNet-1K val set.

on ImageNet-10 and ImageNet-20.

**ImageNet-10  $\leftrightarrow$  ImageNet-20.** In Tab. 4, we compare OOD detection performance tested with ImageNet-10 as the ID dataset and ImageNet-20 as the OOD dataset (ImageNet-10  $\rightarrow$  ImageNet-20), and vice versa (ImageNet-20  $\rightarrow$  ImageNet-10). SUPREME achieves the best performance, with the lowest FPR95 and highest AUROC scores in both scenarios. These results underscore its robustness and reliability in near OOD.

### 5.3. Ablation Study

To understand the effectiveness of SUPREME, we present the average results of an ablation study using CLIP (ViT-B/16) on ImageNet-1k  $\rightarrow$  four OOD datasets. The detailed results are given in the Appendix.

**Effectiveness of the proposed modules (BPG and ITC) and scores ( $S_{GMP}$ ).** In Tab. 5, we evaluate the effectiveness of BPG and ITC, as well as the proposed score  $S_{GMP}$ , for enhancing OOD detection. We see that excluding BPG (-BPG) raises FPR95 to 27.51 and reduces AUROC to 93.71, highlighting BPG’s importance in reducing false positives.

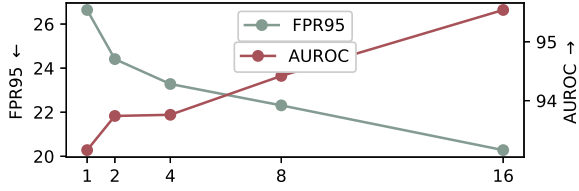


Figure 3. Performance comparison on the length of prompts.

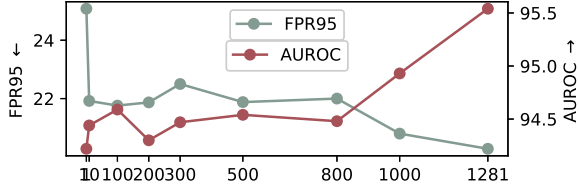


Figure 4. Performance comparison on the number of based images used for obtaining image prototypes. “1281” corresponds to using all the training images as the base images.

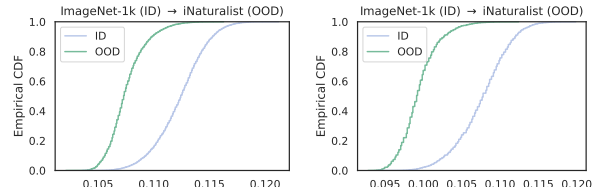
Similarly, removing ITC (-ITC) significantly degrades performance, increasing FPR95 to 28.59 and lowering AUROC to 93.38. Furthermore, when the model uses  $S_{MCM}$  instead of  $S_{GMP}$ , the performance also declines, with FPR95 at 25.03 and AUROC at 94.80. Our full model, incorporating ITC, BPG, and  $S_{GMP}$ , achieves the best overall performance. This demonstrates the combined efficacy of these modules and the proposed OOD score  $S_{GMP}$ .

**SUPREME improves the ID performance.** OOD detection acts as a preliminary step before models make predictions, aiming to perform a binary classification to distinguish between ID and OOD samples. However, it is also important to understand how OOD methods work with ID classification. In Tab. 6, we compare the Top-1 accuracy of different methods on the ImageNet-1K validation set. SUPREME achieves the highest accuracy, reaching 71.8%. Compared to other OOD detection methods, e.g., CLIPN (68.5%) and ID-like (68.3%), SUPREME shows a considerable gain, underscoring its effectiveness in maintaining high ID accuracy while also excelling in OOD detection.

**Impact of the length of prompts.** In the main experiments, we follow previous works [46, 72, 73] and set the length of prompts to  $L = 16$ . Here, we would like to validate that 16 is the best choice for SUPREME. We see in Fig. 3 that among the choices from 1 to 16, 16 obtains the lowest FPR95 and highest AUROC. Increasing the length of prompts improves the OOD detection performance.

**Impact of base image size for constructing ID image prototypes.** In  $S_{GMP}$ , we use a set of base images to construct image prototypes  $\{P_{i,c}\}_{c \in [C]}$ . To understand how the size of base images affects performance, we conduct experiments varying its size. The results in Fig. 4 show that by increasing the number of images for each class, the performance of SUPREME is improved, as image prototypes are closer to the real distribution. FPR95 and AUROC reach the best when using all the images.

**Effectiveness of  $S_{GMP}$ .** To empirically show the effective-



(a)  $S_{MCM}$ ,  $KS = 0.7270$  [45].

(b)  $S_{GMP}$ ,  $KS = 0.8724$ .

Figure 5. Comparison between  $S_{MCM}$  [45] and our  $S_{GMP}$  on ImageNet-1k (ID) to iNaturalist (OOD). The scores are multiplied by 100 for better illustration. “KS” is the statistic from the Kolmogorov–Smirnov test. Higher KS statistic values indicate a greater difference between two distributions. Best viewed in color.

ness of  $S_{GMP}$ , we visualize the empirical cumulative distribution of  $S_{MCM}$  and our  $S_{GMP}$  in Fig. 5. We use our best model trained on ImageNet-1k (ID), with iNaturalist being the OOD dataset.  $S_{GMP}$  clearly improves the gap between ID and OOD data in the empirical CDF figure. Moreover, the statistics of Kolmogorov–Smirnov test is enlarged from 0.7270 ( $S_{MCM}$ ) to 0.8724 ( $S_{GMP}$ ), indicating that using  $S_{GMP}$  has more separable scores compared to  $S_{MCM}$ .

## 6. Conclusion

In this paper, we introduced SUPREME, a novel VLM-based few-shot tuning OOD detection framework designed to minimize the modality gap between text and image in CLIP. SUPREME incorporates two key modules: BPG, which enhances image-text fusion, and ITC, which minimizes the inter- and intra-modal distances. We also proposed the generalized multi-modal prototype OOD score,  $S_{GMP}$ , using multi-modal prototypes and embeddings to improve robustness and reduce false positives. Experimental results show that SUPREME consistently outperforms existing VLM-based OOD detection methods.

**Limitations.** The efficiency of SUPREME partially relies on the introduction of multi-modal prototypes, which may not always be feasible in scenarios with strict data constraints. Exploring more advanced methods such as image generation or retrieval from a web-scale dataset could help alleviate the dependency on the ID data. Moreover, our SUPREME and previous VLM-based methods use CLIP as the base model. It would be interesting to explore the efficacy of using advanced VLMs, such as ImageBind [14], in OOD detection. Finally, in this work we have only explored the effectiveness of multi-modal positive/ID prototypes. Introducing negative/OOD prototypes may further enhance our framework’s versatility.

## References

- [1] Nikolas Adaloglou, Felix Michels, Tim Kaiser, and Markus Kollmann. Adapting Contrastive Language-Image Pre-trained (CLIP) Models for Out-of-Distribution Detection. *Transactions on Machine Learning Research*, 2023. 1



- [2] Yichen Bai, Zongbo Han, Bing Cao, Xiaoheng Jiang, Qinghua Hu, and Changqing Zhang. ID-like Prompt Learning for Few-Shot Out-of-Distribution Detection. In *Proceedings of the IEEE/CVF Conference on Computer Vision and Pattern Recognition*, pages 17480–17489, 2024. 1, 2, 3, 6, 7
- [3] Lukas Bossard, Matthieu Guillaumin, and Luc Van Gool. Food-101 – Mining Discriminative Components with Random Forests. In *European Conference on Computer Vision*, pages 446–461, 2014. 3
- [4] Chentao Cao, Zhun Zhong, Zhanke Zhou, Yang Liu, Tongliang Liu, and Bo Han. Envisioning Outlier Exposure by Large Language Models for Out-of-Distribution Detection. In *ICML*, 2024. 1, 3, 6, 7, 2
- [5] Ting Chen, Simon Kornblith, Mohammad Norouzi, and Geoffrey E. Hinton. A simple framework for contrastive learning of visual representations. In *Proceedings of the 37th International Conference on Machine Learning, ICML 2020, 13-18 July 2020, Virtual Event*, pages 1597–1607. PMLR, 2020. 3
- [6] M. Cimpoi, S. Maji, I. Kokkinos, S. Mohamed, and A. Vedaldi. Describing Textures in the Wild. In *Proceedings of the IEEE Conf. on Computer Vision and Pattern Recognition (CVPR)*, 2014. 5, 6, 4
- [7] Jia Deng, Wei Dong, Richard Socher, Li-Jia Li, Kai Li, and Li Fei-Fei. ImageNet: A large-scale hierarchical image database. In *IEEE Conference on Computer Vision and Pattern Recognition*, pages 248–255, 2009. 2, 5, 6
- [8] Jacob Devlin, Ming-Wei Chang, Kenton Lee, and Kristina Toutanova. BERT: Pre-training of Deep Bidirectional Transformers for Language Understanding. *arXiv:1810.04805 [cs]*, 2019. arXiv: 1810.04805. 3
- [9] Terrance DeVries and Graham W. Taylor. Learning Confidence for Out-of-Distribution Detection in Neural Networks, 2018. arXiv:1802.04865 [stat]. 2
- [10] Xuefeng Du, Yiyun Sun, Jerry Zhu, and Yixuan Li. Dream the Impossible: Outlier Imagination with Diffusion Models. In *Advances in Neural Information Processing Systems*, pages 60878–60901, 2023. 3
- [11] Sepideh Esmailpour, Bing Liu, Eric Robertson, and Lei Shu. Zero-Shot Out-of-Distribution Detection Based on the Pre-trained Model CLIP. In *Proceedings of the AAAI Conference on Artificial Intelligence*, pages 6568–6576, 2022. arXiv:2109.02748 [cs]. 1
- [12] Stanislav Fort, Jie Ren, and Balaji Lakshminarayanan. Exploring the Limits of Out-of-Distribution Detection. In *Advances in Neural Information Processing Systems*, pages 7068–7081. Curran Associates, Inc., 2021. 1, 3, 6, 7
- [13] Zijian Gao, Jingyu Liu, Weiqi Sun, Sheng Chen, Dedan Chang, and Lili Zhao. CLIP2TV: Align, Match and Distill for Video-Text Retrieval, 2022. arXiv:2111.05610 [cs]. 4
- [14] Rohit Girdhar, Alaaeldin El-Nouby, Zhuang Liu, Mannat Singh, Kalyan Vasudev Alwala, Armand Joulin, and Ishan Misra. ImageBind: One Embedding Space To Bind Them All, 2023. arXiv:2305.05665 [cs]. 1, 3, 8
- [15] Tao Guo, Song Guo, and Junxiao Wang. pFedPrompt: Learning Personalized Prompt for Vision-Language Models in Federated Learning. In *Proceedings of the ACM Web Conference 2023*, pages 1364–1374, New York, NY, USA, 2023. Association for Computing Machinery. 3
- [16] Kaiming He, Xiangyu Zhang, Shaoqing Ren, and Jian Sun. Deep Residual Learning for Image Recognition. In *IEEE Conference on Computer Vision and Pattern Recognition*, pages 770–778, Las Vegas, NV, 2016. IEEE Computer Society. 1
- [17] Matthias Hein, Maksym Andriushchenko, and Julian Bitterwolf. Why ReLU Networks Yield High-Confidence Predictions Far Away From the Training Data and How to Mitigate the Problem. In *2019 IEEE/CVF Conference on Computer Vision and Pattern Recognition (CVPR)*, pages 41–50, Long Beach, CA, USA, 2019. IEEE. 2
- [18] Dan Hendrycks and Kevin Gimpel. A Baseline for Detecting Misclassified and Out-of-Distribution Examples in Neural Networks. In *International Conference on Learning Representations*, 2017. 1, 2, 3, 6, 7
- [19] Dan Hendrycks, Mantas Mazeika, and Thomas Dietterich. Deep Anomaly Detection with Outlier Exposure. In *International Conference on Learning Representations*, 2018. 3
- [20] Georg Hess, Adam Tonderski, Christoffer Petersson, Kalle Åström, and Lennart Svensson. LidarCLIP or: How I learned to talk to point clouds. In *Proceedings of the IEEE/CVF winter conference on applications of computer vision (WACV)*, pages 7438–7447, 2024. 1, 3
- [21] Rui Huang and Yixuan Li. MOS: Towards Scaling Out-of-distribution Detection for Large Semantic Space. In *2021 IEEE/CVF Conference on Computer Vision and Pattern Recognition (CVPR)*, pages 8706–8715, Nashville, TN, USA, 2021. IEEE. 1, 3, 6, 7, 4
- [22] Rui Huang, Andrew Geng, and Yixuan Li. On the Importance of Gradients for Detecting Distributional Shifts in the Wild. In *Advances in Neural Information Processing Systems*, pages 677–689. Curran Associates, Inc., 2021. 2, 3
- [23] Wenyu Jiang, Hao Cheng, MingCai Chen, Chongjun Wang, and Hongxin Wei. DOS: Diverse Outlier Sampling for Out-of-Distribution Detection. In *International Conference on Learning Representations*, 2024. 3
- [24] Xue Jiang, Feng Liu, Zhen Fang, Hong Chen, Tongliang Liu, Feng Zheng, and Bo Han. Negative label guided OOD detection with pretrained vision-language models. In *ICLR*, 2024. 1, 3, 6, 7
- [25] K J Joseph, Salman Khan, Fahad Shahbaz Khan, and Vineeth N Balasubramanian. Towards Open World Object Detection. In *2021 IEEE/CVF Conference on Computer Vision and Pattern Recognition (CVPR)*, pages 5826–5836, Nashville, TN, USA, 2021. IEEE. 3
- [26] Omar Khattab and Matei Zaharia. ColBERT: Efficient and Effective Passage Search via Contextualized Late Interaction over BERT, 2020. arXiv:2004.12832 [cs]. 1, 3
- [27] Muhammad Uzair Khattak, Syed Talal Wasim, Muzammal Naseer, Salman Khan, Ming-Hsuan Yang, and Fahad Shahbaz Khan. Self-regulating Prompts: Foundational Model Adaptation without Forgetting. In *International Conference on Computer Vision*, pages 15190–15200, 2023. 3

- [28] Tung Kieu, Bin Yang, and Christian S. Jensen. Outlier Detection for Multidimensional Time Series Using Deep Neural Networks. In *IEEE International Conference on Mobile Data Management*, pages 125–134, Aalborg, Denmark, 2018. IEEE. 3
- [29] Alex Krizhevsky, Ilya Sutskever, and Geoffrey E Hinton. Imagenet classification with deep convolutional neural networks. In *NeurIPS*, pages 1097–1105, 2012. 3
- [30] Kimin Lee, Kibok Lee, Honglak Lee, and Jinwoo Shin. A Simple Unified Framework for Detecting Out-of-Distribution Samples and Adversarial Attacks. In *Advances in Neural Information Processing Systems*. Curran Associates, Inc., 2018. 2, 3
- [31] Brian Lester, Rami Al-Rfou, and Noah Constant. The Power of Scale for Parameter-Efficient Prompt Tuning, 2021. arXiv:2104.08691 [cs]. 3
- [32] Fei-Fei Li, Marco Andreeto, Marc’Aurelio Ranzato, and Pietro Perona. Caltech 101, 2022. 3
- [33] Jingyao Li, Pengguang Chen, Zexin He, Shaozuo Yu, Shu Liu, and Jiaya Jia. Rethinking Out-of-Distribution (OOD) Detection: Masked Image Modeling Is All You Need. In *IEEE Conference on Computer Vision and Pattern Recognition*, pages 11578–11589, 2023. 3
- [34] Jingyao Li, Pengguang Chen, Shaozuo Yu, Shu Liu, and Jiaya Jia. MOODv2: Masked Image Modeling for Out-of-Distribution Detection, 2024. arXiv:2401.02611 [cs]. 3
- [35] Jinglun Li, Xinyu Zhou, Kaixun Jiang, Lingyi Hong, Pinxue Guo, Zhaoyu Chen, Weifeng Ge, and Wenqiang Zhang. TagOOD: A Novel Approach to Out-of-Distribution Detection via Vision-Language Representations and Class Center Learning. In *ACM MM*. arXiv, 2024. arXiv:2408.15566 [cs]. 3
- [36] Tianqi Li, Guansong Pang, Xiao Bai, Wenjun Miao, and Jin Zheng. Learning Transferable Negative Prompts for Out-of-Distribution Detection. In *Proceedings of the IEEE/CVF Conference on Computer Vision and Pattern Recognition*, pages 17584–17594, 2024. 1, 2, 3, 5, 6, 7
- [37] Xiang Lisa Li and Percy Liang. Prefix-Tuning: Optimizing Continuous Prompts for Generation. In *Proceedings of the 59th Annual Meeting of the Association for Computational Linguistics and the 11th International Joint Conference on Natural Language Processing (Volume 1: Long Papers)*, pages 4582–4597, Online, 2021. Association for Computational Linguistics. 3
- [38] Shiyu Liang, Yixuan Li, and R. Srikant. Enhancing The Reliability of Out-of-distribution Image Detection in Neural Networks, 2020. arXiv:1706.02690 [cs]. 1, 3, 6, 7
- [39] Weixin Liang, Yuhui Zhang, Yongchan Kwon, Serena Yeung, and James Zou. Mind the gap: Understanding the modality gap in multi-modal contrastive representation learning. In *Advances in neural information processing systems*, 2022. 1, 2, 4, 5
- [40] Kai Liu, Zhihang Fu, Chao Chen, Sheng Jin, Ze Chen, Mingyuan Tao, Rongxin Jiang, and Jieping Ye. Category-Extensible Out-of-Distribution Detection via Hierarchical Context Descriptions. In *Advances in Neural Information Processing Systems*, pages 33241–33261, 2023. 1, 3, 6, 7
- [41] Weitang Liu, Xiaoyun Wang, John Owens, and Yixuan Li. Energy-based Out-of-distribution Detection. In *Advances in Neural Information Processing Systems*, pages 21464–21475. Curran Associates, Inc., 2020. 1, 2, 3, 6, 7
- [42] Yuyuan Liu, Choubo Ding, Yu Tian, Guansong Pang, Vasileios Belagiannis, Ian Reid, and Gustavo Carneiro. Residual Pattern Learning for Pixel-Wise Out-of-Distribution Detection in Semantic Segmentation. In *International Conference on Computer Vision*, pages 1151–1161, 2023. 3
- [43] Subhansu Maji, Esa Rahtu, Juho Kannala, Matthew Blaschko, and Andrea Vedaldi. Fine-Grained Visual Classification of Aircraft. Technical report, 2013. eprint: 1306.5151. 3
- [44] George A. Miller. WordNet: A lexical database for english. *Communications of The Acm*, 38(11):39–41, 1995. tex.bibsource: dblp computer science bibliography, https://dblp.org tex.timestamp: Fri, 24 Mar 2023 16:31:07 +0100. 1, 3
- [45] Yifei Ming, Ziyang Cai, Jiuxiang Gu, Yiyun Sun, Wei Li, and Yixuan Li. Delving into out-of-distribution detection with vision-language representations. In *Advances in neural information processing systems*, 2022. 1, 2, 3, 4, 5, 6, 7, 8
- [46] Atsuyuki Miyai, Qing Yu, Go Irie, and Kiyoharu Aizawa. LoCoOp: Few-Shot Out-of-Distribution Detection via Prompt Learning. In *Advances in Neural Information Processing Systems*, pages 76298–76310, 2023. 1, 2, 3, 5, 6, 7, 8
- [47] Harikrishna Narasimhan, Aditya Krishna Menon, Wittawat Jitkittum, and Sanjiv Kumar. Plugin estimators for selective classification with out-of-distribution detection. In *International Conference on Learning Representations*, 2024. 2
- [48] Jun Nie, Yonggang Zhang, Zhen Fang, Tongliang Liu, Bo Han, and Xinmei Tian. Out-of-Distribution Detection with Negative Prompts. In *ICLR*, 2024. 1, 3, 6, 7
- [49] OpenAI. GPT-4 Technical Report, 2023. arXiv:2303.08774 [cs]. 1, 3
- [50] Jaewoo Park, Yoon Gyo Jung, and Andrew Beng Jin Teoh. Nearest Neighbor Guidance for Out-of-Distribution Detection. In *2023 IEEE/CVF International Conference on Computer Vision (ICCV)*, pages 1686–1695, Paris, France, 2023. IEEE. 2
- [51] Sangha Park, Jisoo Mok, Dahuin Jung, Saehyung Lee, and Sungroh Yoon. On the Powerfulness of Textual Outlier Exposure for Visual OoD Detection. In *Advances in Neural Information Processing Systems*, pages 51675–51687, 2023. 1
- [52] Omkar M. Parkhi, Andrea Vedaldi, Andrew Zisserman, and C. V. Jawahar. Cats and Dogs. In *IEEE Conference on Computer Vision and Pattern Recognition*, 2012. 3
- [53] Alec Radford, Jong Wook Kim, Chris Hallacy, Aditya Ramesh, Gabriel Goh, Sandhini Agarwal, Girish Sastry, Amanda Askell, Pamela Mishkin, Jack Clark, Gretchen Krueger, and Ilya Sutskever. Learning Transferable Visual Models From Natural Language Supervision. In *Proceedings of the 38th International Conference on Machine Learning*, pages 8748–8763. PMLR, 2021. ISSN: 2640-3498. 1, 3, 6

- [54] Taylor Shin, Yasaman Razeghi, Robert L. Logan IV, Eric Wallace, and Sameer Singh. AutoPrompt: Eliciting Knowledge from Language Models with Automatically Generated Prompts, 2020. arXiv:2010.15980 [cs]. 3
- [55] Yiyou Sun, Chuan Guo, and Yixuan Li. ReAct: Out-of-distribution Detection With Rectified Activations. In *Advances in Neural Information Processing Systems*, pages 144–157. Curran Associates, Inc., 2021. 2, 3, 1
- [56] Yiyou Sun, Yifei Ming, Xiaojin Zhu, and Yixuan Li. Out-of-Distribution Detection with Deep Nearest Neighbors. In *Proceedings of the 39th International Conference on Machine Learning*, pages 20827–20840. PMLR, 2022. ISSN: 2640-3498. 1, 2, 6, 7
- [57] Leitian Tao, Xuefeng Du, Jerry Zhu, and Yixuan Li. Non-parametric Outlier Synthesis. In *ICLR*, 2023. 6, 7
- [58] Michael Tschannen, Basil Mustafa, and Neil Houlsby. CLIPPO: Image-and-Language Understanding from Pixels Only, 2023. arXiv:2212.08045 [cs]. 4
- [59] Grant Van Horn, Oisín Mac Aodha, Yang Song, Yin Cui, Chen Sun, Alex Shepard, Hartwig Adam, Pietro Perona, and Serge Belongie. The iNaturalist Species Classification and Detection Dataset. In *2018 IEEE/CVF Conference on Computer Vision and Pattern Recognition*, pages 8769–8778, Salt Lake City, UT, 2018. IEEE. 5, 6, 4
- [60] Haoqi Wang, Zhizhong Li, Litong Feng, and Wayne Zhang. ViM: Out-of-distribution with virtual-logit matching. In *Proceedings of the IEEE/CVF conference on computer vision and pattern recognition (CVPR)*, pages 4921–4930, 2022. 1, 3, 6, 7
- [61] Hualiang Wang, Yi Li, Hui Feng Yao, and Xiaomeng Li. CLIPN for Zero-Shot OOD Detection: Teaching CLIP to Say No. In *2023 IEEE/CVF International Conference on Computer Vision (ICCV)*, pages 1802–1812, Paris, France, 2023. IEEE. 1, 3, 6, 7
- [62] Hongxin Wei, Renchunzi Xie, Hao Cheng, Lei Feng, Bo An, and Yixuan Li. Mitigating Neural Network Overconfidence with Logit Normalization, 2022. Version Number: 2. 2
- [63] Jianxiong Xiao, James Hays, Krista A. Ehinger, Aude Oliva, and Antonio Torralba. SUN database: Large-scale scene recognition from abbey to zoo. In *2010 IEEE Computer Society Conference on Computer Vision and Pattern Recognition*, pages 3485–3492, San Francisco, CA, USA, 2010. IEEE. 5, 6, 4
- [64] Mingyu Xu, Zheng Lian, Bin Liu, and Jianhua Tao. VRA: Variational Rectified Activation for Out-of-distribution Detection. In *Advances in Neural Information Processing Systems*, 2023. 2
- [65] Jing Kang Yang, Pengyun Wang, Dejian Zou, Zitang Zhou, Kunyuan Ding, Wenxuan Peng, Haoqi Wang, Guangyao Chen, Bo Li, Yiyou Sun, Xuefeng Du, Kaiyang Zhou, Wayne Zhang, Dan Hendrycks, Yixuan Li, and Ziwei Liu. OpenOOD: Benchmarking Generalized Out-of-Distribution Detection, 2022. Version Number: 1. 1, 2
- [66] Jing Kang Yang, Kaiyang Zhou, Yixuan Li, and Ziwei Liu. Generalized Out-of-Distribution Detection: A Survey, 2024. arXiv:2110.11334 [cs]. 3
- [67] Hantao Yao, Rui Zhang, and Changsheng Xu. Visual-Language Prompt Tuning with Knowledge-Guided Context Optimization. In *2023 IEEE/CVF Conference on Computer Vision and Pattern Recognition (CVPR)*, pages 6757–6767, Vancouver, BC, Canada, 2023. IEEE. 3
- [68] Jingyang Zhang, Jing Kang Yang, Pengyun Wang, Haoqi Wang, Yueqian Lin, Haoran Zhang, Yiyou Sun, Xuefeng Du, Kaiyang Zhou, Wayne Zhang, Yixuan Li, Ziwei Liu, Yiran Chen, and Hai Li. OpenOOD v1.5: Enhanced Benchmark for Out-of-Distribution Detection, 2023. arXiv:2306.09301 [cs]. 2
- [69] Yabin Zhang, Wenjie Zhu, Chenhang He, and Lei Zhang. LAPT: Label-driven Automated Prompt Tuning for OOD Detection with Vision-Language Models. In *ECCV*. arXiv, 2024. arXiv:2407.08966 [cs]. 1, 3
- [70] Bolei Zhou, Agata Lapedriza, Aditya Khosla, Aude Oliva, and Antonio Torralba. Places: A 10 Million Image Database for Scene Recognition. *IEEE Transactions on Pattern Analysis and Machine Intelligence*, 40(6):1452–1464, 2018. 5, 6, 4
- [71] Da-Wei Zhou, Han-Jia Ye, and De-Chuan Zhan. Learning Placeholders for Open-Set Recognition. In *2021 IEEE/CVF Conference on Computer Vision and Pattern Recognition (CVPR)*, pages 4399–4408, Nashville, TN, USA, 2021. IEEE. 3
- [72] Kaiyang Zhou, Jing Kang Yang, Chen Change Loy, and Ziwei Liu. Conditional prompt learning for vision-language models. In *IEEE/CVF conference on computer vision and pattern recognition (CVPR)*, 2022. 3, 6, 7, 8
- [73] Kaiyang Zhou, Jing Kang Yang, Chen Change Loy, and Ziwei Liu. Learning to Prompt for Vision-Language Models. *International Journal of Computer Vision*, 130(9):2337–2348, 2022. 3, 5, 6, 7, 8

# Mitigating the Modality Gap: Few-Shot Out-of-Distribution Detection with Multi-modal Prototypes and Image Bias Estimation

## Supplementary Material

In this Appendix, we present the details and complete results corresponding to Tab. 1 in Sec. 7.1, additional ablation studies in Sec. 7.2, benchmark dataset specifications in Sec. 7.3, and the proof of Theorem 1 in Sec. 8.

## 7. Experiments

### 7.1. Empirical Evidence for RQ1

Methods	FPR95 (%) ↓	AUROC (%) ↑
ImageNet-100 → iNaturalist		
$S_{MCM}$ [45]	18.13	96.77
$S_{MMP}$ (Ours, Eq. (4))	<b>14.76</b>	<b>97.36</b>
ImageNet-100 → SUN		
$S_{MCM}$ [45]	36.45	<b>94.54</b>
$S_{MMP}$ (Ours, Eq. (4))	<b>30.28</b>	92.51
ImageNet-100 → Places		
$S_{MCM}$ [45]	34.52	<b>94.36</b>
$S_{MMP}$ (Ours, Eq. (4))	<b>34.04</b>	93.92
ImageNet-100 → Texture		
$S_{MCM}$ [45]	41.22	92.25
$S_{MMP}$ (Ours, Eq. (4))	<b>17.66</b>	<b>96.66</b>

Table 7. Comparison of OOD detection results on four OOD tasks. We use CLIP-B/16 for  $S_{MCM}$  and  $S_{MMP}$  (ours, Eq. (4)). FPR95 represents the false positive rate of OOD images when the true positive rate of ID images is at 95% while AUROC is the area under the receiver operating characteristic curve. Best in **bold**.

To empirically justify the effectiveness of multi-modal (image and text) prototypes, we present experiments using  $S_{MCM}$  and  $S_{MMP}$  on four OOD datasets (*i.e.*, iNaturalist, SUN, Places, and Texture). We use CLIP-B/16 as the base model for  $S_{MCM}$  and  $S_{MMP}$ . All the training images from ImageNet-100 are used for generating image prototypes.

Our method,  $S_{MMP}$ , consistently demonstrates superior performance in terms of FPR95 across all four tasks, achieving the lowest values, with notable improvements on iNaturalist (14.76 vs. 18.13) and Texture (17.66 vs. 41.22), highlighting its robustness in reducing false positives. For AUROC,  $S_{MMP}$  achieves the highest score on iNaturalist (97.36) and Texture (96.66). However, in SUN and Places datasets, while  $S_{MMP}$  maintains competitive performance, it slightly underperforms  $S_{MCM}$  in AUROC (92.51 vs. 94.54 on SUN and 93.92 vs. 94.36 on Places).

Overall, the results underscore the effectiveness of  $S_{MMP}$  and multi-modal prototypes in reducing false positives and

the performance of VLM-based OOD detection.

### 7.2. Ablations

To understand the effectiveness of SUPREME, we present the results of several ablation studies using CLIP (ViT-B/16) on ImageNet-1k → four OOD datasets (*i.e.*, iNaturalist, SUN, Places, and Texture). Our experiments examine the effectiveness of the proposed components (*i.e.*, ITC, BPG, and  $S_{GMP}$ ), the impact of combining SUPREME with post-hoc methods, training data efficiency (number of shots), the statistical evaluation of  $S_{GMP}$ , and sensitivity to hyperparameters.

**Evaluating the effectiveness of the proposed modules (BPG and ITC) and  $S_{GMP}$  (complete results).** To evaluate the effectiveness of the proposed modules and  $S_{GMP}$ , we present detailed results of a combinatorial ablation study in Tab. 8. Performance is evaluated across four datasets (*i.e.*, iNaturalist, SUN, Places, and Texture).

Compared with the base model (MCM [45]), introducing ITC considerably reduces FPR95 to 28.29 while boosting AUROC to 93.40. Similarly, BPG improves performance, though to a slightly lesser extent, achieving an average FPR95 of 29.89 and AUROC of 93.07. When ITC and BPG are combined, the performance improves further, reaching an average FPR95 of 25.03 and AUROC of 94.80. These results show that both ITC and BPG individually contribute substantial improvements over the base model, while their combination yields even greater performance.

For the proposed score,  $S_{GMP}$ , when combining it with either ITC or BPG, the performance shows incremental gains compared to using ITC or BPG alone. The best results are obtained when all three components (ITC, BPG, and  $S_{GMP}$ ) are combined, yielding an average FPR95 of 20.28 and AUROC of 95.54. This configuration achieves the lowest FPR95 and highest AUROC across all configurations and datasets.

**Combining SUPREME with post-hoc methods.** To understand how SUPREME combines with existing representative post-hoc methods, *i.e.*, ReAct [55] and  $S_{EOE}$  [4], we present a systematic study in Tab. 9. We directly apply ReAct and  $S_{EOE}$  on our best model as post-hoc methods, which means we do not use them during training. For ReAct, we set the threshold at 0.95, while for  $S_{EOE}$ , we follow the standard parameters. We see that using ReAct alone makes the performance worse with average FPR95 of 21.21 and AUROC of 94.35. On the other hand,  $S_{EOE}$  boosts average FPR95 from 20.28 to 19.25. When combining ReAct

ITC	BPG	$S_{GMP}$	ImageNet-1k $\rightarrow$ OOD Datasets								Average	
			iNaturalist		SUN		Places		Texture		FPR95 $\downarrow$	AUROC $\uparrow$
			FPR95 $\downarrow$	AUROC $\uparrow$	FPR95 $\downarrow$	AUROC $\uparrow$	FPR95 $\downarrow$	AUROC $\uparrow$	FPR95 $\downarrow$	AUROC $\uparrow$		
			30.91	94.61	37.59	92.57	44.69	89.77	57.77	86.11	42.74	90.77
✓			14.64	96.76	22.92	95.01	33.05	91.86	42.55	90.00	28.29	93.40
	✓		18.75	96.15	24.47	94.43	33.36	91.80	42.96	89.92	29.89	93.07
✓	✓		20.00	96.02	22.35	95.65	28.19	93.82	29.57	93.82	25.03	94.80
✓		✓	12.73	97.27	23.86	94.80	33.65	91.67	39.80	91.10	27.51	93.71
	✓	✓	15.78	96.79	24.56	94.23	33.35	91.55	40.66	90.93	28.59	93.38
✓	✓	✓	<b>8.27</b>	<b>98.29</b>	<b>19.40</b>	<b>95.84</b>	<b>26.69</b>	<b>93.56</b>	<b>26.77</b>	<b>94.45</b>	<b>20.28</b>	<b>95.54</b>

Table 8. Effectiveness of different modules and the proposed OOD score  $S_{GMP}$ . When  $S_{GMP}$  is not combined with BPG, it degenerates to  $S_{MMP}$ .

ReAct	$S_{EOE}$	ImageNet-1k $\rightarrow$ OOD Datasets								Average	
		iNaturalist		SUN		Places		Texture		FPR95 $\downarrow$	AUROC $\uparrow$
		FPR95 $\downarrow$	AUROC $\uparrow$	FPR95 $\downarrow$	AUROC $\uparrow$	FPR95 $\downarrow$	AUROC $\uparrow$	FPR95 $\downarrow$	AUROC $\uparrow$		
		8.27	98.29	19.40	95.84	26.69	<b>93.56</b>	<b>26.77</b>	<b>94.45</b>	20.28	<b>95.54</b>
✓		10.73	97.32	14.22	96.23	<b>24.12</b>	93.03	35.76	90.83	21.21	94.35
	✓	4.83	98.89	<b>13.02</b>	<b>96.91</b>	24.58	93.22	34.57	92.34	19.25	95.34
✓	✓	<b>4.28</b>	<b>99.00</b>	13.63	96.72	24.40	93.51	34.24	92.20	<b>19.14</b>	95.36

Table 9. Performance of SUPREME combined with post-hoc methods, *i.e.*, ReAct [55] and  $S_{EOE}$  [4].

Methods	Parameters	Trainable Parameters	Image Prototypes	Inference
MCM	124,323,841	0	-	$O(1)$
SUPREME	124,891,683 ( $\uparrow$ 567,842)	567,842	$O(N_{base})$	$O(1)$

Table 10. Comparison of (trainable) parameters and inference efficiency between MCM and SUPREME with the base model as CLIP-B/16.

and  $S_{EOE}$ , the FPR95 is boosted to 19.14 on average. However, using ReAct and/or  $S_{EOE}$  decreases the average AUROC compared to vanilla SUPREME, showing that these post-hoc methods might only help reduce false positives. The experiments show that SUPREME is compatible with these post-hoc methods without performance drops.

**Computational cost of the training and inference.** Table 10 compares parameter efficiency and inference scalability between the baseline MCM method and our proposed SUPREME, using CLIP-B/16 as the base model. While both methods exhibit comparable total parameter sizes, SUPREME introduces 567,842 trainable parameters to achieve its enhanced functionality, representing a negligible increase of 0.46% in total parameters. SUPREME obtains image prototypes with a complexity of  $O(N_{base})$ , while maintaining inference complexity at  $O(1)$  given one test input. Also, the calculation of image prototypes can be conducted before inference, and image prototypes can be shared among all the test samples, which avoids introducing overhead during inference compared with MCM. It demonstrates the scalability of SUPREME without computational overhead during inference, effectively addressing challenges of learnable flexibility and inference efficiency.

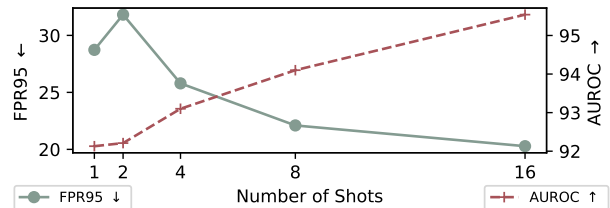


Figure 6. The impact of different sizes of fine-tuning data.

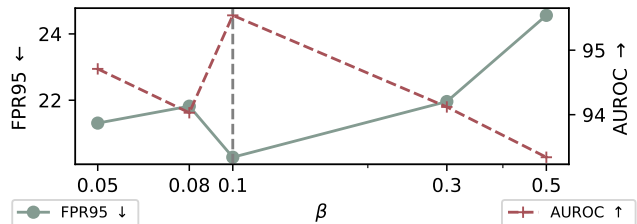
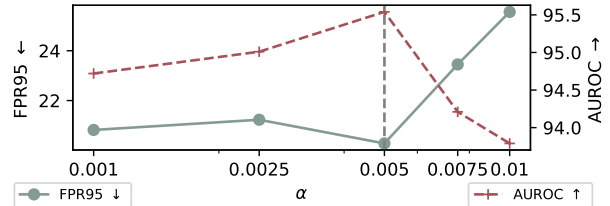


Figure 7. Hyperparameter sensitivity ( $\alpha$  and  $\beta$ ). We report the average FPR95 and AUROC.

**How much data do we need for few-shot tuning?** We evaluate the effect of the number of shots for few-shot tuning on the model’s performance in Fig. 6. As the number

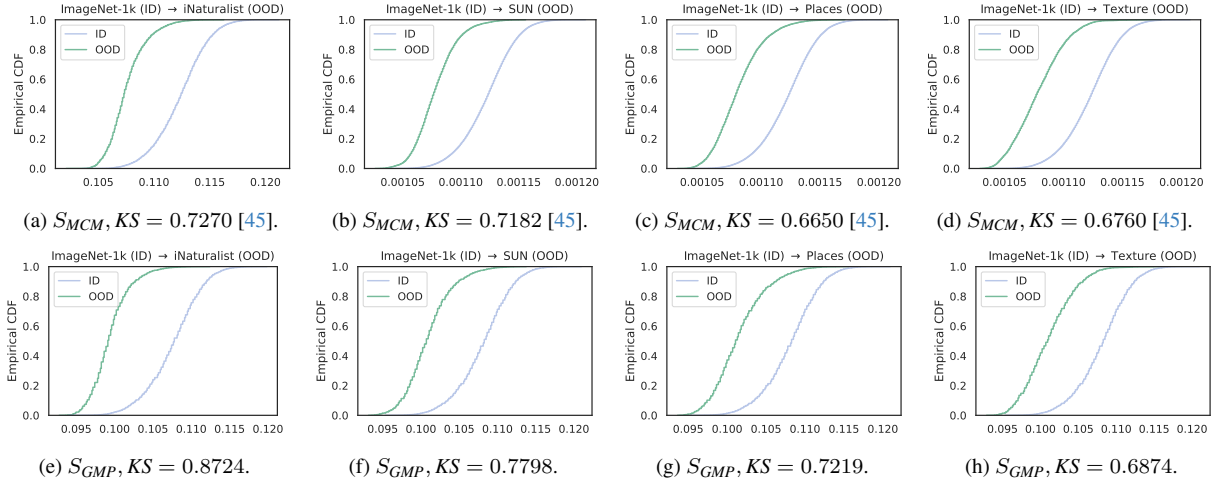


Figure 8. The comparison between  $S_{MCM}$  [45] and our proposed  $S_{GMP}$  score (Eq. (11)) on ImageNet-1k (ID) to four OOD datasets, *i.e.*, iNaturalist, SUN, Places, and Texture. Best viewed in color.

of shots increases from 1 to 16, we observe a consistent improvement in both metrics. Specifically, FPR95 decreases from 28.73 at 1-shot to 20.28 at 16-shot, indicating that more shots lead to better separability between ID and OOD data. Similarly, AUROC improves from 92.13 at 1-shot to a peak of 95.54 at 16-shot, demonstrating enhanced overall detection performance. These results highlight the robustness of SUPREME in leveraging additional labeled examples, with diminishing returns on FPR95 as data size increases. While higher shot numbers provide the best performance, the model performs reasonably well even with a limited number of shots, showcasing its flexibility in low-data scenarios.

**Hyperparameter ( $\alpha$  and  $\beta$ ) sensitivity.** We analyze the effect of the trade-off hyperparameters  $\alpha$  and  $\beta$  (Sec. 4.2) on the model’s performance, as shown in Fig. 7. For  $\alpha$ , we observe a trade-off between FPR95 and AUROC as its value increases. Specifically, as  $\alpha$  grows from 0.001 to 0.01, FPR95 decreases initially from 20.82 to 20.28 at  $\alpha = 0.005$ , indicating improved separability, but then rises to 25.56 at  $\alpha = 0.01$ . Meanwhile, AUROC peaks at 95.54 for  $\alpha = 0.005$  before declining, indicating that excessively large values of  $\alpha$  may overemphasize certain features, leading to diminished overall performance. Similarly,  $\beta$  demonstrates a comparable trend. The FPR95 achieves its lowest value of 20.28 at  $\beta = 0.1$ , while AUROC peaks at 95.54. The results of both hyperparameters suggest that SUPREME is not sensitive to the parameters and that moderate values ( $\alpha = 0.005, \beta = 0.1$ ) balance the trade-off between false positive rate and overall discriminative ability.

**Full statistical evaluation of  $S_{GMP}$ .** We visualize the empirical cumulative distribution (empirical CDF) and the Kolmogorov–Smirnov (KS) test statistics for  $S_{MCM}$  and

our proposed  $S_{GMP}$  in Fig. 8. The evaluation uses our best model trained on the ImageNet-1k (ID) dataset, with iNaturalist, SUN, Places, and Texture serving as OOD datasets. The empirical CDF clearly shows that  $S_{GMP}$  improves the gap between ID and OOD data more effectively. Furthermore, the KS test statistics improve considerably from 0.7270, 0.7182, 0.6650, and 0.6760 ( $S_{MCM}$ ) to 0.8724, 0.7798, 0.7219, and 0.6874 ( $S_{GMP}$ ) across the four OOD datasets. These results indicate that  $S_{GMP}$  achieves better separation between ID and OOD scores compared to  $S_{MCM}$ .

### 7.3. Details of Benchmarking Datasets

**ImageNet-100, ImageNet-10, and ImageNet-20.** Following MCM [45], we choose 100/10/20 classes from ImageNet-1k [29] to form ImageNet-100, ImageNet-10, and ImageNet-20. The chosen classes for each dataset are as follows:

- **ImageNet-100:** n03877845, n03000684, n03110669, n03710721, n02825657, n02113186, n01817953, n04239074, n02002556, n04356056, n03187595, n03355925, n03125729, n02058221, n01580077, n03016953, n02843684, n04371430, n01944390, n03887697, n04037443, n02493793, n01518878, n03840681, n04179913, n01871265, n03866082, n03180011, n01910747, n03388549, n03908714, n01855032, n02134084, n03400231, n04483307, n03721384, n02033041, n01775062, n02808304, n13052670, n01601694, n04136333, n03272562, n03895866, n03995372, n06785654, n02111889, n03447721, n03666591, n04376876, n03929855, n02128757, n02326432, n07614500, n01695060, n02484975, n02105412, n04090263, n03127925,

n04550184, n04606251, n02488702, n03404251,  
n03633091, n02091635, n03457902, n02233338,  
n02483362, n04461696, n02871525, n01689811,  
n01498041, n02107312, n01632458, n03394916,  
n04147183, n04418357, n03218198, n01917289,  
n02102318, n02088364, n09835506, n02095570,  
n03982430, n04041544, n04562935, n03933933,  
n01843065, n02128925, n02480495, n03425413,  
n03935335, n02971356, n02124075, n07714571,  
n03133878, n02097130, n02113799, n09399592,  
n03594945.

- **ImageNet-10:** n04552348, n04285008, n01530575,  
n02123597, n02422699, n02107574, n01641577,  
n03417042, n02389026, n03095699.

- **ImageNet-20:** n04147183, n02951358, n02782093,  
n04389033, n03773504, n02917067, n02317335,  
n01632458, n01630670, n01631663, n02391049,  
n01693334, n01697457, n02120079, n02114367,  
n02132136, n03785016, n04310018, n04266014,  
n04252077.

**Other datasets.** Similarly, we use subsets from iNaturalist [59], SUN [63], Places [70], and Texture [6] as OOD datasets, which are created by Huang and Li [21].

- **iNaturalist** contains images from the natural world with images from 5089 classes, belonging to 13 super-categories, such as Plantae (Plant), Insecta (Insect), Aves (Bird), Mammalia (Mammal). The subset containing 110 plant classes not present in ImageNet-1k is chosen as the OOD test set. The classes are as follows, *Coprosma lucida*, *Cucurbita foetidissima*, *Mitella diphylla*, *Selaginella bigelovii*, *Toxicodendron vernix*, *Rumex obtusifolius*, *Ceratophyllum demersum*, *Streptopus amplexifolius*, *Portulaca oleracea*, *Cynodon dactylon*, *Agave lechuguilla*, *Pennantia corymbosa*, *Sapindus saponaria*, *Prunus serotina*, *Chondracanthus exasperatus*, *Sambucus racemosa*, *Polypodium vulgare*, *Rhus integrifolia*, *Woodwardia areolata*, *Epifagus virginiana*, *Rubus idaeus*, *Croton setiger*, *Mammillaria dioica*, *Opuntia littoralis*, *Cercis canadensis*, *Psidium guajava*, *Asclepias exaltata*, *Linaria purpurea*, *Ferocactus wislizeni*, *Briza minor*, *Arbutus menziesii*, *Corylus americana*, *Pleopeltis polypodioides*, *Myoporum laetum*, *Persea americana*, *Avena fatua*, *Blechnum discolor*, *Physocarpus capitatus*, *Ungnadia speciosa*, *Cercocarpus betuloides*, *Arisaema dracontium*, *Juniperus californica*, *Euphorbia prostrata*, *Leptopteris hymenophylloides*, *Arum italicum*, *Raphanus sativus*, *Myrsine australis*, *Lupinus stiversii*, *Pinus echinata*, *Geum macrophyllum*, *Ripogonum scandens*, *Echinocereus triglochidiatus*, *Cupressus macrocarpa*, *Ulmus crassifolia*, *Phormium tenax*, *Aptenia cordifolia*, *Osmunda claytoniana*, *Datura wrightii*, *Solanum rostratum*, *Viola adunca*, *Toxicodendron diversilobum*, *Viola sororia*, *Uropappus lindleyi*, *Veronica chamaedrys*, *Ade-*

*nocaulon bicolor*, *Clintonia uniflora*, *Cirsium scariosum*, *Arum maculatum*, *Taraxacum officinale officinale*, *Orthilia secunda*, *Eryngium yuccifolium*, *Diodia virginiana*, *Cuscuta gronovii*, *Sisyrinchium montanum*, *Lotus corniculatus*, *Lamium purpureum*, *Ranunculus repens*, *Hirschfeldia incana*, *Phlox divaricata laphamii*, *Lilium martagon*, *Clarkia purpurea*, *Hibiscus moscheutos*, *Polanisia dodecandra*, *Fallugia paradoxa*, *Oenothera rosea*, *Proboscidea louisianica*, *Packera glabella*, *Impatiens parviflora*, *Glaucium flavum*, *Cirsium andersonii*, *Heliopsis helianthoides*, *Hesperis matronalis*, *Callirhoe pedata*, *Crocasmia × crocosmiiflora*, *Calochortus albus*, *Nuttallanthus canadensis*, *Argemone albiflora*, *Eriogonum fasciculatum*, *Pyrrhopappus pauciflorus*, *Zantedeschia aethiopica*, *Melilotus officinalis*, *Peritoma arborea*, *Sisyrinchium bellum*, *Lobelia siphilitica*, *Sorghastrum nutans*, *Typha domingensis*, *Rubus laciniatus*, *Dichelostemma congestum*, *Chimaphila maculata*, *Echinocactus texensis*.

- **SUN** contains 899 classes that cover indoor, urban, and natural places. We use the subset that contains 50 natural objects that do not overlap with ImageNet-1k. The classes we use are *badlands*, *bamboo forest*, *bayou*, *botanical garden*, *canal (natural)*, *canal (urban)*, *catacomb*, *cavern (indoor)*, *corn field*, *creek*, *crevasse*, *desert (sand)*, *desert (vegetation)*, *field (cultivated)*, *field (wild)*, *fishpond*, *forest (broadleaf)*, *forest (needleleaf)*, *forest path*, *forest road*, *hayfield*, *ice floe*, *ice shelf*, *iceberg*, *islet*, *marsh*, *ocean*, *orchard*, *pond*, *rainforest*, *rice paddy*, *river*, *rock arch*, *sky*, *snowfield*, *swamp*, *tree farm*, *trench*, *vineyard*, *waterfall (block)*, *waterfall (fan)*, *waterfall (plunge)*, *wave*, *wheat field*, *herb garden*, *putting green*, *ski slope*, *topiary garden*, *vegetable garden*, *formal garden*.
- **Places** contains photos labeled with scene semantic categories from three macro-classes: Indoor, Nature, and Urban. We use a subset sampled from 50 categories that are not present in ImageNet-1k. The classes we use are *badlands*, *bamboo forest*, *canal (natural)*, *canal (urban)*, *corn field*, *creek*, *crevasse*, *desert (sand)*, *desert (vegetation)*, *desert road*, *field (cultivated)*, *field (wild)*, *field road*, *forest (broadleaf)*, *forest path*, *forest road*, *formal garden*, *glacier*, *grotto*, *hayfield*, *ice floe*, *ice shelf*, *iceberg*, *igloo*, *islet*, *japanese garden*, *lagoon*, *lawn*, *marsh*, *ocean*, *orchard*, *pond*, *rainforest*, *rice paddy*, *river*, *rock arch*, *ski slope*, *sky*, *snowfield*, *swamp*, *swimming hole*, *topiary garden*, *tree farm*, *trench*, *tundra*, *underwater (ocean deep)*, *vegetable garden*, *waterfall*, *wave*, *wheat field*.
- **Texture** contains images of textures and abstracted patterns. As no categories overlap with ImageNet1k, we use the entire dataset.

## 8. Proof of Theorem 1

We first introduce three necessary assumptions before proceeding with the proof of our theorem.

**Assumption 1** (ID image embeddings follow the distribution centered at ID image prototypes). *Image embeddings  $\mathbf{x}_c$  are drawn from the symmetric distribution  $\mathcal{D}_c$  which is centered at the image prototypes  $P_{i,c}$  in the embedding space.*

**Assumption 2** (The image-text modality gap exists). *The image embeddings are closer to the ground truth class's image prototypes than the text prototypes due to the modality gap.*

**Remark.** *These two assumptions are the basic assumptions about the multi-modal prototypes and the modality gap. Based on the findings from a recent study [39], these two hold true for most real-world scenarios.*

**Assumption 3** (Models are well trained). *Cosine similarity between embeddings from the same class distribution  $\mathcal{D}_i$  is higher on average than between embeddings from different distributions. And the image embeddings from the  $c$ -th class are equally dissimilar to other classes.*

**Remark.** *Here we only consider the optimal representation extractors without any other assumptions on the models.*

**Assumption 4** (OOD embeddings are not sampled from any ID distribution.). *OOD image embeddings  $\mathbf{x}_{OOD}$  are drawn from a distribution  $\mathcal{D}_{OOD}$  different from any  $\mathcal{D}_c^*$ ,  $\forall c \in [C]$ ,  $* \in [text, image]$ . Besides, the OOD image embeddings are equally similar to all ID text/image classes.*

**Remark.** *This assumption is a general basic assumption on the OOD data, which provides us with an overall characteristic of the OOD data.*

Under the above assumptions, we first would like to prove the following inequality holds,

$$\begin{aligned} \Delta_{\text{image}} &= \mathbb{E} \left[ \max_{i \in [C]} \sigma_i^{\text{image}}(\mathbf{x}_{ID}) - \max_{i \in [C]} \sigma_i^{\text{image}}(\mathbf{x}_{OOD}) \right] \\ &\geq \Delta_{\text{text}} = \mathbb{E} \left[ \max_{i \in [C]} \sigma_i^{\text{text}}(\mathbf{x}_{ID}) - \max_{i \in [C]} \sigma_i^{\text{text}}(\mathbf{x}_{OOD}) \right], \\ \text{s.t. } \sigma_i^* &= \frac{\exp(s_{*,i})}{\sum_{k=1}^N \exp(s_k)}, s_{*,i} = \cos(\mathbf{x}, P_{*,i}), \\ &* \in [image, text], \end{aligned} \quad (12)$$

where  $\mathbf{x}_{ID}$  and  $\mathbf{x}_{OOD}$  are samples from any ID distributions and OOD samples.

First, for ID samples, with Assumption 3, we have

$$\begin{aligned} \mathbb{E} \left[ \max_{c \in [C]} \sigma_c^*(\mathbf{x}_{ID}) \right] &= \frac{\exp(\mu_{\text{intra}}^*)}{\exp(\mu_{\text{intra}}^*) + (C-1) \exp(\mu_{\text{inter}}^*)}, \\ &\forall * \in \{text, image\}, \end{aligned} \quad (13)$$

where  $\mu_{\text{intra}}^* = \max_{c \in [C]} \mathbb{E}[\cos(\mathbf{x}_{ID}, P_{*,c})]$ ,  $\mu_{\text{inter}}^* = \mathbb{E}[\cos(\mathbf{x}_{ID}, I_{c_j})]$ ,  $\forall c_j \in [C] \setminus \{c_{ID}\}$ , and  $C_{ID}$  is the ground-truth class for the input  $\mathbf{x}_{ID}$ .

With assumption 4, for OOD samples, we have,

$$\mathbb{E} \left[ \max_{c \in [C]} \sigma_c^{\text{image}}(\mathbf{x}_{OOD}) \right] = \mathbb{E} \left[ \max_{c \in [C]} \sigma_c^{\text{text}}(\mathbf{x}_{OOD}) \right] = \frac{1}{C}. \quad (14)$$

Then we have,

$$\Delta_{\text{image}} = \mathbb{E} \left[ \max_{c \in [C]} \sigma_c^{\text{image}}(\mathbf{x}_i) \right] - \frac{1}{C}. \quad (15)$$

Similarly, we have,

$$\Delta_{\text{text}} = \mathbb{E} \left[ \max_{c \in [C]} \sigma_c^{\text{text}}(\mathbf{x}_i) \right] - \frac{1}{C}. \quad (16)$$

Since  $\mu_{\text{intra}}^{\text{image}} > \mu_{\text{intra}}^{\text{text}}$  (Assumption 2), we have,

$$\Delta_{\text{image}} > \Delta_{\text{text}}. \quad (17)$$

By simple algebra, we have,

$$\begin{aligned} &\mathbb{E} \left[ \frac{\max_{i \in [C]} \sigma_i^{\text{image}}(\mathbf{x}_{ID}) + \max_{i \in [C]} \sigma_i^{\text{text}}(\mathbf{x}_{ID})}{2} \right. \\ &\quad \left. - \frac{\max_{i \in [C]} \sigma_i^{\text{image}}(\mathbf{x}_{OOD}) + \max_{i \in [C]} \sigma_i^{\text{text}}(\mathbf{x}_{OOD})}{2} \right] \\ &\geq \mathbb{E} \left[ \max_{i \in [C]} \sigma_i^{\text{text}}(\mathbf{x}_{ID}) - \max_{i \in [C]} \sigma_i^{\text{text}}(\mathbf{x}_{OOD}) \right], \\ &\quad \mathbb{E} [S_{MMP}(\mathbf{x}_{ID}) - S_{MMP}(\mathbf{x}_{OOD})] \\ &\geq \mathbb{E} [S_{MCM}(\mathbf{x}_{ID}) - S_{MCM}(\mathbf{x}_{OOD})]. \end{aligned} \quad (18)$$

Now, we complete the proof.